Nuclear Science and Techniques (2026) 37:60
https://doi.org/10.1007/s41365-026-01896-4

Studies of directed flow with event plane method in the HIRFL-CSR external-target experiment

Wan-Long Wu[1,2] · Xiong-Hong He[2,3,4] · Yan-Yu Ren[1] · Di-Yu Shen[2,3,4] · Shu-Su Shi[5] · Xu Sun[2,3,4]

Received: 31 March 2025 / Revised: 30 April 2025 / Accepted: 21 May 2025 / Published online: 28 January 2026

Abstract
The Cooling-Storage-Ring External-target Experiment (CEE) at the Heavy Ion Research Facility in Lanzhou (HIRFL) is designed to study the properties of nuclear matter created in heavy-ion collisions at beam energies from a few hundred MeV/u up to 1 GeV/u. It aims to facilitate research on the quantum chromodynamics (QCD) phase structure in the high-baryon-density region. Collective flow is a fundamental observable in heavy-ion collision experiments, providing information on the bulk properties of the produced matter. Although the standard event plane method has been widely used to measure collective flow, it is still important to validate and optimize this method for the CEE spectrometer. In this paper, we study the experimental procedures for measuring directed flow in ^{238}U + ^{238}U collisions at 500 MeV/u, using event planes reconstructed by Multi-Wire Drift Chamber and Zero Degree Calorimeter, respectively. Jet AA Microscopic (JAM) transport generator is used to generate events, and the detector response is simulated by the CEE Fast Simulation (CFS) package. Finally, the optimal kinematic region for proton directed flow measurements is discussed for the future CEE experiment.

Keywords Heavy-ion collisions · CEE · Directed flow · Event plane

1 Introduction

Quantum chromodynamics (QCD) predicts a transition from hadronic matter to deconfined quark–gluon matter at sufficiently high temperature and/or high density [1, 2]. Heavy-ion collision experiments at the Relativistic Heavy Ion Collider (RHIC) and the Large Hadron Collider (LHC) have provided unique experimental evidence for this transition [3–8]. While striking progress has been made in the past decades, some foundational questions remain to be determined, such as the existence of a critical end point in the QCD phase diagram and the equation of state of nuclear matter at baryon densities much larger than the saturation density [9, 10]. At HIRFL-CSR energies, a hadronic gas with densities reaches 2–3 times nuclear saturation density, where temperatures around 40 MeV can be produced [11]. Experiments at these energies are vital to elucidate the properties of QCD in the low-temperature and high-baryon-density region [12–15].

The CEE spectrometer is designed to measure charged particles in the fixed target heavy-ion collisions at HIRFL-CSR [16]. It is the first comprehensive nuclear physics experiment research facility in the GeV energy range in China [11]. With various types of ion beam provided by HIRFL-CSR, e.g., ^{12}C + ^{12}C at 1.1 GeV/u ($\sqrt{s_{\rm NN}}$ = 2.36 GeV) and ^{238}U + ^{238}U at 500 MeV/u ($\sqrt{s_{\rm NN}}$ = 2.1 GeV) [17, 18], CEE spectrometer is an ideal platform to explore the QCD phase diagram in the high-baryon-density region, to

This work was supported in part by the National Key R&D Program of China (No. 2024YFA1610700) and the National Natural Science Foundation of China (No. 12475147).

✉ Xu Sun
xusun@impcas.ac.cn

[1] School of Physics, Harbin Institute of Technology, Harbin 150001, China

[2] Institute of Modern Physics, Chinese Academy of Sciences, Lanzhou 730000, China

[3] School of Nuclear Science and Technology, University of Chinese Academy of Sciences, Beijing 100049, China

[4] State Key Laboratory of Heavy Ion Science and Technology, Institute of Modern Physics, Chinese Academy of Sciences, Lanzhou 730000, China

[5] Key Laboratory of Quark & Lepton Physics (MOE) and Institute of Particle Physics, Central China Normal University, Wuhan 430079, China

study the nuclear matter equation of state and to search for the existence of the critical end point.

Collective flow is one of the most important observables in relativistic heavy-ion collision experiments for studying the bulk behavior of the created matter [19]. The azimuthal anisotropy of emitted particles in the momentum space can be expanded in a Fourier series [20]:

$$E\frac{\mathrm{d}^3N}{\mathrm{d}p^3} = \frac{1}{2\pi}\frac{\mathrm{d}^2N}{p_\mathrm{T}\mathrm{d}p_\mathrm{T}\mathrm{d}y}\left(1+\sum_{n=1}^{\infty}2v_n\cos\left(n\left(\phi-\Psi_\mathrm{RP}\right)\right)\right), \tag{1}$$

where Ψ_{RP} is the azimuthal angle of reaction plane defined by the beam direction and impact parameter. The Fourier coefficients $v_n = \langle\cos[n(\phi_i - \Psi_{\mathrm{RP}})]\rangle$ are the nth-order flow coefficient, and the bracket means the average over all particles and events. The first harmonic (v_1) is referred to as directed flow, found to be sensitive to the compressibility of dense matter [21, 22].

The reaction plane angle is not directly measurable in the heavy-ion collision experiment, but one can use the observed event plane angle Ψ_{EP} from the anisotropic flow itself as an estimate on an event-by-event basis. This is the *standard event plane method* [23]. This approach has been widely applied in collective flow analyses over the past decades [24–31], yet it remains crucial to optimize it for the CEE experiment and to ensure a reliable collective flow signal.

This paper is organized as follows. Section 2 describes the setup of CEE detector and the simulation tools. Section 3 presents the reconstruction and correction method of event plane from different sub-detectors of CEE experiment. Section 4 discusses the results of proton v_1 simulated ^{238}U + ^{238}U collisions at $\sqrt{s_{\mathrm{NN}}} = 2.1$ GeV. A summary is presented in Sect. 5.

2 CEE detector and fast simulation

The CEE spectrometer is designed for charged particle reconstruction in HIRFL-CSR energy region [12, 32]. Figure 1 presents the primary detector configurations. The main components of CEE spectrometer are as follows: a large-gap dipole magnet with a 0.5 T magnetic field along the y-axis [33, 34]; a Time Projection Chamber (TPC) [35, 36] system consisting of two identical TPCs surrounded by the inner Time-of-Flight (iToF) [37, 38] detectors located in the mid-rapidity region; three layers of Multi-Wire Drift Chamber (MWDC) [39–42] followed by the external Time-of-Flight (eToF) [43, 44] detectors and Zero Degree Calorimeter (ZDC) [45, 46] in the forward region; the start time (T0) [47, 48] detector; and a silicon pixel beam monitor (BM) [49, 50], which are installed on

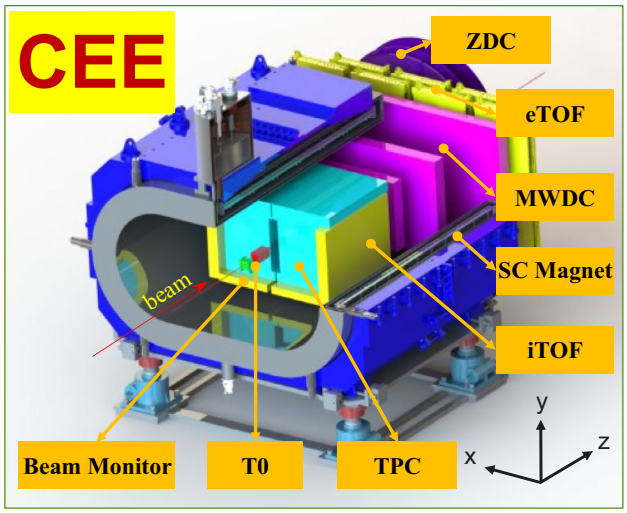

Fig. 1 (Color online) Sketch of CEE detector [16]

the beam line in the upstream side of the target to track the beam position. The target is placed at (0, 0, −35) cm to maximize the pion acceptance for ^{238}U + ^{238}U collisions at $\sqrt{s_{\mathrm{NN}}} = 2.1$ GeV, where the (0, 0, 0) cm is set to the center of TPC geometry. The magnetic field from the dipole magnet is along the y-axis, causing the beam and final-state charged particles to bend along the x-axis. Detectors in the forward region, such as eToF and ZDC, are shifted along the x-axis accordingly to allow the beam to pass through their hollow centers, as shown in Fig. 1. In this paper, the JAM model [51, 52] is used to generate simulated events of ^{238}U + ^{238}U collisions at $\sqrt{s_{\mathrm{NN}}} = 2.1$ GeV followed by CFS package to simulate the CEE experiment.

In JAM, the initial position of nucleon is sampled according to the distribution of nuclear density. All hadronic states, including resonances, are propagated in space–time with explicit trajectories. Inelastic hadron–hadron collisions are described using two approaches: At low energies, resonance production dominates, while at high energies, the color string picture becomes the primary mechanism. The model includes two modes: cascade and mean field. In the cascade mode, hadrons and their excited states follow straight trajectories in two-body collisions. The nuclear mean-field mode incorporates the interactions of hadrons with the nuclear medium and the equation of state, which is implemented based on the relativistic quantum molecular dynamics approach (RQMD) [53, 54].

The final-state particles generated by the JAM model are processed through the CEE Fast Simulation (CFS) framework. This framework simulates the CEE detector environment and produces responses for all CEE subdetectors. The CFS enhances computational efficiency through parametric modeling and analytically derived

formulations, which collectively simulate critical sub-detector characteristics such as detector acceptance, momentum resolution, energy deposition, and particle flight time. Each sub-system's resolution effects are implemented via Gaussian smearing of the true input values. This methodology systematically accounts for measurement uncertainties while maintaining an optimal computational efficiency.

Figure 2 shows the proton acceptance of TPC, MWDC, and ZDC for events with impact parameter 5 fm $< b <$ 6 fm from JAM + CFS simulation. The top panel of Fig. 2 shows the angular coverage of TPC (Fig. 2a) and MWDC (Fig. 2b) and the spatial coverage of ZDC (Fig. 2c). The CEE spectrometer covers polar angles from 10° to 120° in the laboratory frame, corresponding to proton rapidities between -0.7 and 1 in the center-of-mass frame. A clear efficiency loss in TPC azimuth at 90° and 270° is shown in Fig. 2a, which is due to the two-half design of TPC [36]. Figure 2c shows the two-dimensional $X-Y$ hit distribution on ZDC. Clearly, the left side ($X < 0$) of ZDC receives more hits than the right side ($X \geq 0$). This is because the final-state charged particles are deflected by the magnetic field (along the y-axis), making them more likely to hit one side of ZDC [55]. The bottom panel of Fig. 2 shows the kinematic coverage of TPC, MWDC and ZDC. The dashed box in Fig. 2d indicates the kinematic range (0.2 GeV/c< p_T < 0.7 GeV/c and $-0.5 < y < 0.5$) used for the directed flow simulation of charged particles measured by TPC. Further details are discussed in Sect. 4.

3 Event plane reconstruction with MWDC and ZDC

The reaction plane in heavy-ion collisions is defined by the beam direction and impact parameter, which is not directly measurable. In the experiment, one uses the azimuthal emission angles of detected particles to determine the event plane [23], which is used to estimate the reaction plane. The nth-order event plane angle, Ψ_n, is calculated by the nth-order flow vector $\boldsymbol{Q}_n$. In this study, we focus on simulating v_1, because its magnitude is significantly larger than that of the higher-order flow coefficients at CEE energy. The 1st-order flow vector $\boldsymbol{Q}_1$ and the event plane angle Ψ_1 are defined as

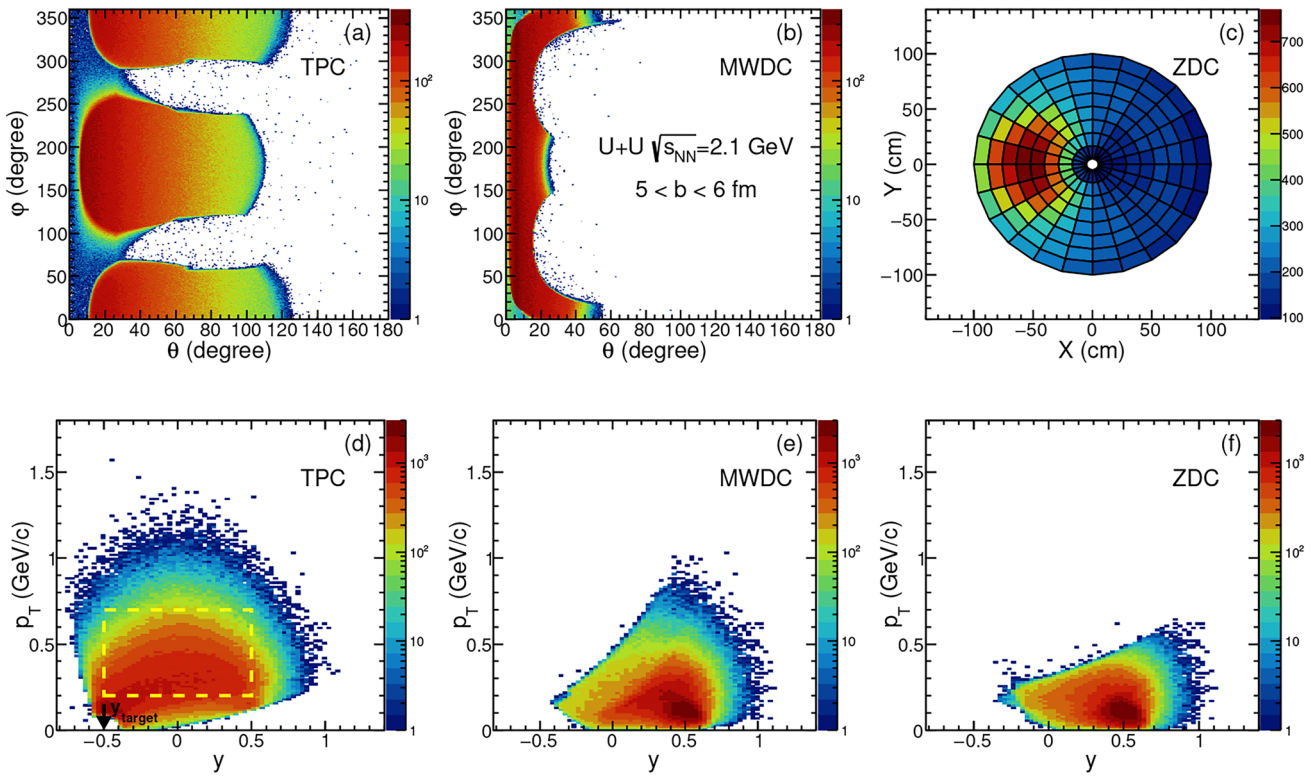

Fig. 2 (Color online) Simulated proton acceptance from CFS package for 2.1 GeV ^{238}U + ^{238}U collisions with 5 fm $< b <$ 6 fm. Top panel: proton track/hit distribution in TPC (**a**), MWDC (**b**), and ZDC (**c**); bottom panel: proton kinematic acceptance in TPC (**d**), MWDC (**e**), and ZDC (**f**). The dashed rectangle in panel (**d**) indicates the kinematic region used for the proton v_1 analysis

$$\boldsymbol{Q}_1 = \begin{pmatrix} Q_{x,1} \\ Q_{y,1} \end{pmatrix} = \begin{pmatrix} \sum_i \omega_i \cos(\phi_i) \\ \sum_i \omega_i \sin(\phi_i) \end{pmatrix},$$
$$\Psi_1 = \tan^{-1} \frac{Q_{y,1}}{Q_{x,1}}, \tag{2}$$

where the sum is over all particles used in the event plane determination and ω_i are weights to optimize the event plane resolution.

The main detectors used for event plane reconstruction in the CEE experiment are MWDC and ZDC. Since the MWDC is a track-based detector and the ZDC is a hit-based detector, the information used to obtain the $\boldsymbol{Q}_1$ and the correction procedure are different.

For the track-based MWDC, the ϕ_i used in Eq. (2) denotes the azimuthal angle of the i-th particle (obtained from the particle's momentum) in the event plane determination and ω_i is p_T of the i-th particle. The reaction plane distribution should be isotropic. Due to the finite detector efficiency and acceptance, the detected particles are azimuthally anisotropic in the laboratory system which leads to an anisotropic distribution of the reconstructed event plane [19, 23]. The black line in Fig. 3a presents the raw Ψ_1 distribution observed from the MWDC.

To correct the effect of anisotropic Ψ_1 distribution, the re-centering correction is applied [56]. The first-order flow vector $\boldsymbol{Q}_1$ is recalculated by subtracting the $(Q_{x,1}, Q_{y,1})$ values averaged over all events, as described by

$$\boldsymbol{q}_{\text{rec}} = \begin{pmatrix} q_{x,\text{rec}} \\ q_{y,\text{rec}} \end{pmatrix} = \begin{pmatrix} \langle \cos(\phi_i) \rangle \\ \langle \sin(\phi_i) \rangle \end{pmatrix},$$
$$\boldsymbol{Q}_1 = \begin{pmatrix} \sum_i \omega_i (\cos(\phi_i) - q_{x,\text{rec}}) \\ \sum_i \omega_i (\sin(\phi_i) - q_{y,\text{rec}}) \end{pmatrix}, \tag{3}$$

where the $\boldsymbol{q}_{\text{rec}}$ is obtained by averaging over all particles used in event plane determination from all events.

The re-centered Ψ_1 distribution from MWDC is not perfectly uniform as shown by the red line in Fig. 3a. The remaining anisotropic structure is corrected by shift procedure [57]. For each event, a shift angle $\Delta\Psi_1$ is calculated from the following equation:

$$\Psi_1' = \Delta\Psi_1 + \Psi_1,$$
$$\Delta\Psi_1 = \sum_{i=1}^{n} \frac{2}{i} \left[-\langle \sin(i\Psi_1) \rangle \cos(i\Psi_1) + \langle \cos(i\Psi_1) \rangle \sin(i\Psi_1) \right], \tag{4}$$

where n is the maximum correction order and the brackets refer to the average over the events used in event plane reconstruction. Ψ_1 is the event plane angle after re-centering correction, and Ψ_1' is the event plane angle after the shift correction. As indicated by the blue line in Fig. 3a, an isotropic event plane distribution is obtained after the shift correction.

For the hit-based ZDC, the ϕ_i used in Eq. (2) denotes the azimuthal angle in the laboratory frame of the i-th particle hit on the ZDC and ω_i is the energy deposition ΔE of the i-th particle in the ZDC [55]. The magnetic field direction of the CEE experiment is along the y-axis which is perpendicular to the beam direction. The final-state charged particles are deflected by the magnetic field, therefore, more likely to hit on one side of the ZDC, as shown in Fig. 2c. This acceptance asymmetry of the ZDC will bias the reconstructed event plane toward a π azimuth, as shown by the black line in Fig. 3b. To correct for this acceptance bias caused by the magnetic field, Ref. [55] proposed a position weight correction to calibrate the asymmetric acceptance as defined in Eq. (5):

$$w_i = \Delta E \times P,$$
$$P = \begin{cases} n(-x, y, \Delta E)/n(x, y, \Delta E) & x < 0, \\ 1 & x > 0, \end{cases} \tag{5}$$

where the weight w_i is defined as the deposited energy ΔE of the i-th particle hit on the ZDC, multiplied by a position

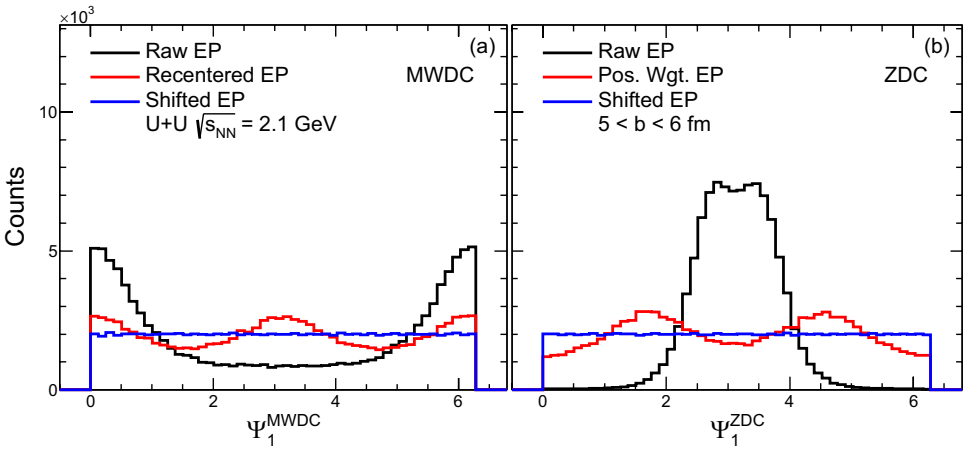

Fig. 3 (Color online) **a** 1st-order event plane distribution reconstructed by MWDC for raw distribution (black line), after re-centering correction (red line) and after re-centering + shift correction (blue line); **b** 1st-order event plane distribution reconstructed by ZDC for raw distribution (black line), after position weight correction (red line) and after position weight + shift correction (blue line)

weight factor derived from the two-dimensional $X-Y$ hit distribution. This position weight is calculated by the ratio of the number of hits on the right side of ZDC to that on the left, or to those on the left, using ΔE as the weighting factor [54]. A shift correction is also applied after the position weight correction because the event plane distribution is not perfectly uniform, shown by the red line in Fig. 3b. The shift angle is calculated from Eq. (4), where Ψ_1 is the position weight-corrected event plane angle, and Ψ_1' is the event plane angle after shift calibration. The resulting distribution, achieved after applying all corrections, is shown by the blue line in Fig. 3b. Due to the finite multiplicity of final-state particles, the reconstructed event plane deviates from the true reaction plane. We correct for this deviation using the first-order event plane resolution defined in Eq. (6):

$$R_1 = \left\langle \cos(\Psi_{1,\mathrm{EP}} - \Psi_{\mathrm{RP}}) \right\rangle. \tag{6}$$

Since the Ψ_{RP} is not directly measurable, the first-order event plane resolution from MWDC and ZDC is extracted with two-sub-event plane method [19, 23]. In this approach, each event is randomly divided into two sub-events with equal tracks (MWDC) or hits (ZDC). The event plane resolution of the two-sub-event is calculated by

$$R_{1,\mathrm{sub}} = \sqrt{\left\langle \cos\left(\Psi^a_{1,\mathrm{EP}} - \Psi^b_{1,\mathrm{EP}}\right) \right\rangle}, \tag{7}$$

where $\Psi^a_{1,\mathrm{EP}}$ and $\Psi^b_{1,\mathrm{EP}}$ are the corrected event plane angle of two sub-events. Then the full event plane resolution is calculated from Eq. (8):

$$R_1 = \frac{\sqrt{\pi}}{2}\chi_1 e^{(-\chi_1^2/2)}\left(I_0(\chi_1^2/2) + I_1(\chi_1^2/2)\right), \tag{8}$$

where I_0 and I_1 are the modified Bessel functions and $\chi_1 = v_1\sqrt{M}$ which is proportional to the square root of event multiplicity. Thus, the full event plane resolution is obtained by $R_{1,\mathrm{full}} = R_1(\sqrt{2}\chi_{1,\mathrm{sub}})$ [23, 55].

Figure 4 presents the first-order event plane resolution as a function of impact parameter for the MWDC and ZDC, obtained using the two-sub-event method. The resolution from the MWDC is generally higher than that from the ZDC. Both detectors can achieve a maximum resolution ($\sim 90\%$ for MWDC and $\sim 70\%$ for ZDC) in the mid-central collisions (5 fm $< b <$ 7 fm). While the absolute resolution values can vary with different input models, the MWDC consistently shows a better first-order event plane resolution than the ZDC. An important observation is the lack of MWDC event plane resolution data for the most central collisions (0 fm $< b <$ 1 fm). This absence is primarily due to significant non-flow effects, which induce a negative correlation between the two MWDC sub-events. Although this effect can generally be corrected in simulation, such a correction is beyond the scope of this paper.

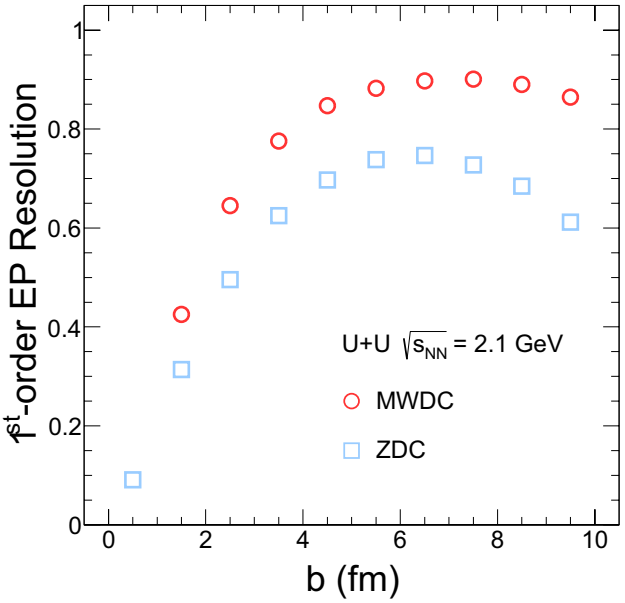

Fig. 4 (Color online) 1st-order event plane resolution as a function of impact parameter b from MWDC and ZDC

4 Directed flow simulation from TPC

With the corrected event plane from MWDC (ZDC) and the corresponding event plane resolution, the directed flow of charged particles detected by TPC is calculated with Eq. (9):

$$v_1 = \left\langle \cos(\phi_i^{\mathrm{TPC}} - \Psi_{1,\mathrm{EP}}) \right\rangle / R_1, \tag{9}$$

where ϕ_i^{TPC} is the azimuth angle of the particle of interest (POI) in the TPC and the bracket denotes the average of all POIs within selected kinematic range in all events with the same event category. In this study, we select the events with impact parameter 5 fm $< b <$ 6 fm for illustration and protons (POIs) within 0.2 GeV/$c <$ $p_{\mathrm{T}} <$ 0.7 GeV/c and $-0.5 < y < 0.5$, indicated by the dashed box in Fig. 2d.

Figure 5 compares the proton v_1 calculated using the true reaction plane versus the event planes reconstructed by different detectors. We first validated the CEE detector's ability to measure the proton v_1 signal by comparing the flow calculated with the true reaction plane (v_1^{RP}) to the theoretical expectation from the JAM model (v_1^{truth}). Their close agreement, shown in Fig. 5a, confirms the detector's fundamental reliability. We then evaluated v_1 using the *standard event plane method* from both the MWDC (v_1^{MWDC}) and ZDC (v_1^{ZDC}). As shown in Fig. 5b and c, after applying corrections for self-correlation and momentum conservation [19, 23,

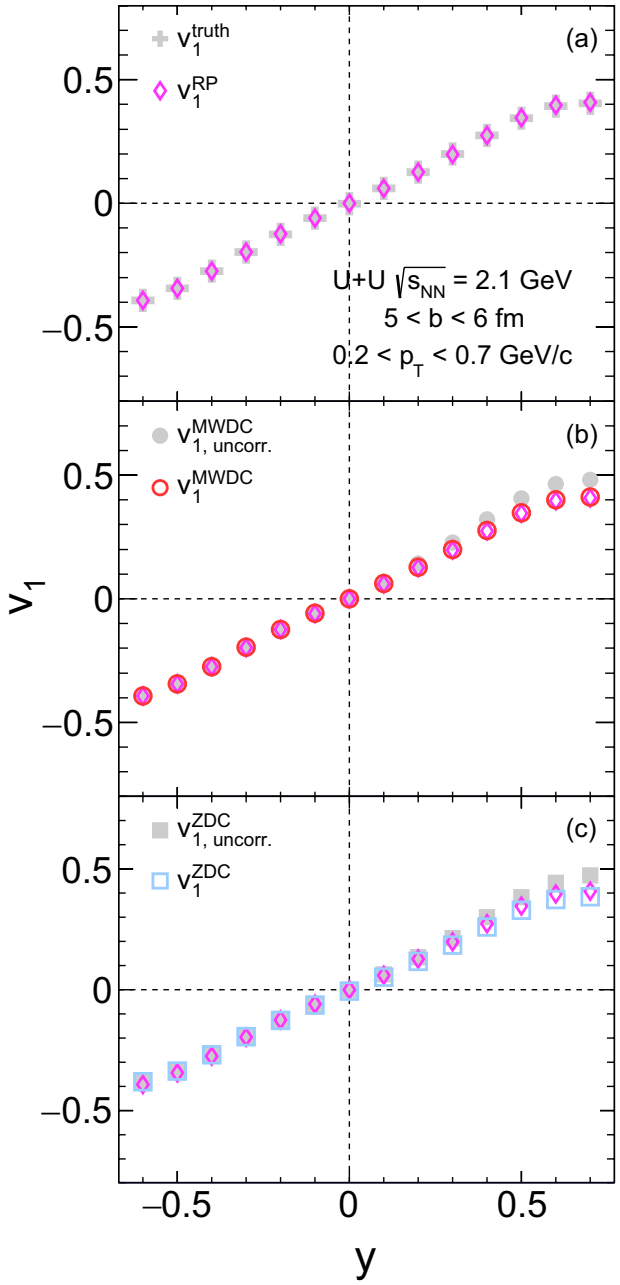

Fig. 5 (Color online) Proton v_1 as a function of rapidity extracted from different detectors: **a** proton v_1 from JAM model (gray cross) and v_1 extracted from reaction plane from CFS package (magenta open diamonds); **b** un-corrected proton v_1 (gray filled circles) and corrected proton v_1 (red open circles, corrected for self-correlation and momentum conservation effect) from 1st-order MWDC event plane; **c** un-corrected proton v_1 (gray filled squares) and corrected proton v_1 (blue open squares, corrected for self-correlation) from 1st-order ZDC event plane

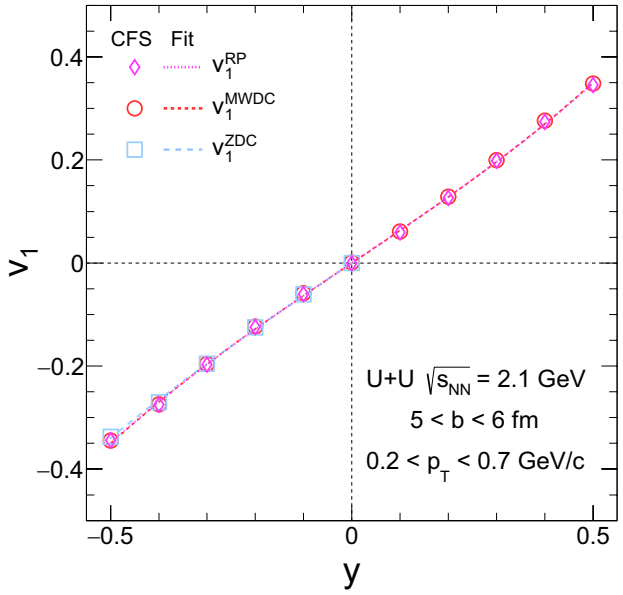

Fig. 6 (Color online) Comparison of proton v_1 extracted from reaction plane (magenta open diamonds), 1st-order MWDC event plane (red open circles), and 1st-order ZDC event plane (blue open squares). The dashed lines are fits to proton v_1 extracted from corresponding planes. The fit function is $y = ax + bx^3$

58], both v_1^{MWDC} and v_1^{ZDC} are consistent with v_1^{RP}. This final result demonstrates that the *standard event plane method* is valid and applicable for directed flow measurements in the CEE experiment.

It is worth noting that the removal of self-correlation and momentum conservation effect is on a track-by-track basis [19, 23, 58], which is achievable by carefully matching reconstructed tracks from MWDC and TPC. But for ZDC, given the complicated magnetic field and the position of ZDC, it is difficult to do a precise matching between ZDC hits and TPC/MWDC tracks. Thus, it is complicated to remove such effects for v_1^{ZDC}. To avoid self-correlation and momentum conservation effect, we propose using the ZDC event plane ($\Psi_{1,\mathrm{EP}}^{\mathrm{ZDC}}$) exclusively for backward protons ($-0.5 < y < 0$) detected in the TPC. The results of this proposed measurement are shown in Fig. 6. The dashed lines are fits to extract v_1 slope, and the fit function is $y = ax + bx^3$. The $\mathrm{d}v_1/\mathrm{d}y$ is 0.631 ± 0.002 for v_1^{RP}, 0.629 ± 0.003 for v_1^{MWDC}, and 0.634 ± 0.012 for v_1^{ZDC}, respectively. The v_1 slopes extracted from v_1^{MWDC} and v_1^{ZDC} are consistent with that from v_1^{RP} within 1σ, which means the proposed measurement is reasonable.

Furthermore, to study the influence of detector effect on the flow measurement, detector efficiency is introduced into the CFS package. A 90% detection efficiency is applied to the TPC, MWDC, and ZDC. Figure 7 displays the results for 100% (symbols) and 90% (bands) for clarity. The consistency between v_1 obtained with 100% and 90% efficiency indicates that the influence of detector

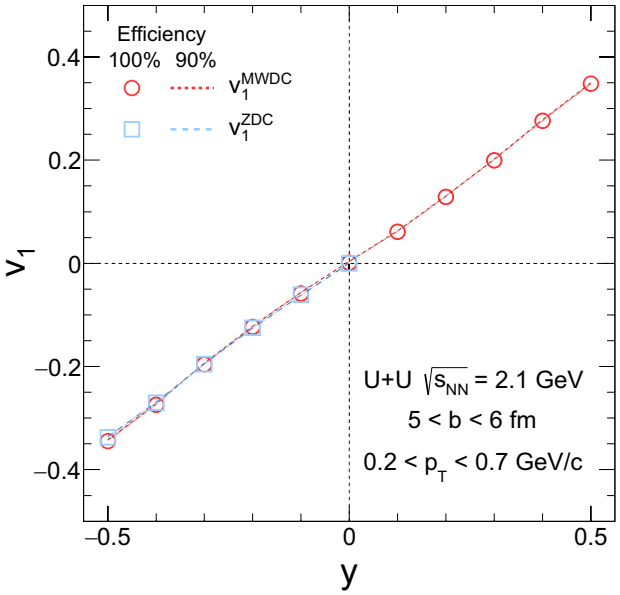

Fig. 7 (Color online) Comparison of proton v_1 with different detector efficiency. Open symbols are proton v_1 extracted with 100% efficiency from MWDC (red open circles) and ZDC (blue open squares). Dashed lines are proton v_1 extracted with 90% efficiency from MWDC (red dashed line) and ZDC (blue dashed line)

efficiency is negligible for flow measurement. It should be noted that a complete study would require applying a realistic, detector-specific efficiency; however, this is not expected to alter the general conclusion.

5 Summary

In summary, we have presented a procedure for simulating directed flow using the *standard event plane method* in the CEE experiment. The JAM model (500 MeV/u ^{238}U + ^{238}U) is used as input for the simulation, and the CFS package is applied to incorporate the CEE detector environment. The directed flow signal is extracted by correlating charged particles detected in the TPC with the first-order event plane reconstructed by the MWDC and ZDC. The paper also discusses the corresponding correction procedures for both the event plane and the resulting v_1. The consistency among v_1^{MWDC}, v_1^{ZDC}, v_1^{RP}, and v_1^{truth} indicated validity of *standard event plane method* in the CEE experiment. We also propose an optimal kinematic region for v_1 measurement using 1st-order event plane reconstructed by MWDC and ZDC. The framework developed in this work can serve as a guideline for directed flow measurements in future CEE experiments.

Acknowledgements We express our appreciation to Chuan Fu, Qi-Chun Feng, Lei Huo, Qiang Hu, Li-Ke Liu, Hua Pei, Hao Qiu, Yaping Wang, Nu Xu, Jing-Bo Zhang, and Ya-Peng Zhang for insightful discussion.

Author contributions All authors contributed to the study conception and design. Material preparation, data collection, and analysis were performed by Wan-Long Wu, Xu Sun, and Yan-Yu Ren. The first draft of the manuscript was written by Wan-Long Wu, and all authors commented on previous versions of the manuscript. All authors read and approved the final manuscript.

Data availability The data that support the findings of this study are openly available in Science Data Bank at https://cstr.cn/31253.11.sciencedb.j00186.00851 and https://www.doi.org/10.57760/sciencedb.j00186.00851.

Declarations

Conflict of interest The authors declare that they have no conflict of interest.

References

1. C. Hartnack, Z.X. Li, L. Neise et al., Quantum molecular dynamics: a microscopic model from UNILAC to CERN energies. Nucl. Phys. A **495**, 303C-320C (1989). https://doi.org/10.1016/0375-9474(89)90328-X
2. E.V. Shuryak, Quark-gluon plasma and hadronic production of leptons, photons and psions. Phys. Lett. B **78**, 150 (1978). https://doi.org/10.1016/0370-2693(78)90370-2
3. I. Arsene, I. Bearden, D. Beavis et al., Quark–gluon plasma and color glass condensate at RHIC? The perspective from the BRAHMS experiment. Nucl. Phys. A **757**, 1–27 (2005). https://doi.org/10.1016/j.nuclphysa.2005.02.130
4. B. Back, M. Baker, M. Ballintijn et al., The PHOBOS perspective on discoveries at RHIC. Nucl. Phys. A **757**, 28–101 (2005). https://doi.org/10.1016/j.nuclphysa.2005.03.084
5. J. Adams, M. Aggarwal, Z. Ahammed et al., Experimental and theoretical challenges in the search for the quark gluon plasma: the STAR Collaboration's critical assessment of the evidence from RHIC collisions. Nucl. Phys. A **757**, 102–183 (2005). https://doi.org/10.1016/j.nuclphysa.2005.03.085
6. K. Adcox, S. Adler, S. Afanasiev et al., Formation of dense partonic matter in relativistic nucleus–nucleus collisions at RHIC: experimental evaluation by the PHENIX collaboration. Nucl. Phys. A **757**, 184–283 (2005). https://doi.org/10.1016/j.nuclphysa.2005.03.086
7. H. Song, Y. Zhou, K. Gajdosova, Collective flow and hydrodynamics in large and small systems at the LHC. Nucl. Sci. Tech. **28**, 99 (2017). https://doi.org/10.1007/s41365-017-0245-4
8. N. Yu, Z.M. Zhang, H.G. Xu et al., Effect of light nuclei on chemical freeze-out parameters at RHIC energies. Nucl. Sci. Tech. **36**, 65 (2025). https://doi.org/10.1007/s41365-025-01661-z
9. X. Luo, N. Xu, Search for the QCD critical point with fluctuations of conserved quantities in relativistic heavy-ion collisions at RHIC: an overview. Nucl. Sci. Tech. **28**, 112 (2017). https://doi.org/10.1007/s41365-017-0257-0
10. J.H. Chen, X. Dong, X.H. He et al., Properties of the QCD matter: review of selected results from the relativistic heavy ion collider beam energy scan (RHIC BES) program. Nucl. Sci. Tech. **35**, 214 (2024). https://doi.org/10.1007/s41365-024-01591-2

11. L. Lü, H. Yi, Z. Xiao et al., Conceptual design of the HIRFL-CSR external-target experiment. Sci. China Phys. Mech. Astron. **60**, 012021 (2017). https://doi.org/10.1007/s11433-016-0342-x
12. D. Guo, X. He, P. Li et al., Studies of nuclear equation of state with the HIRFL-CSR external-target experiment. Eur. Phys. J. A **60**, 36 (2024). https://doi.org/10.1140/epja/s10050-024-01245-2
13. A.K. Sahoo, X. He, Y. Nara et al., Bulk properties of the system formed in U+U collisions at $\sqrt{s_{\rm NN}} = 2.12$ GeV using the jet *AA* microscopic transport mode. Phys. Rev. C **109**, 054902 (2024). https://doi.org/10.1103/PhysRevC.109.054902
14. Z. Ye, H. Zhang, Y. Zhang et al., New Chinese facilities for short-range correlation physics. Eur. Phys. J. A **60**, 126 (2024). https://doi.org/10.1140/epja/s10050-024-01343-1
15. S.W. Lan, S.S. Shi, Anisotropic flow in high baryon density region. Nucl. Sci. Tech. **33**, 21 (2022). https://doi.org/10.1007/s41365-022-01006-0
16. D. Hu, X. Wang, M. Shao et al., Design and performance testing of a T0 detector for the CSR external-target experiment. Nucl. Instrum. Methods A **1057**, 168773 (2023). https://doi.org/10.1016/j.nima.2023.168773
17. J. Xia, W. Zhan, B. Wei et al., The heavy ion cooler-storage-ring project (HIRFL-CSR) at Lanzhou. Nucl. Instrum. Methods A **488**, 11–25 (2002). https://doi.org/10.1016/S0168-9002(02)00475-8
18. L.J. Mao, W.Y.J.C. Yang et al., Introduction of the Heavy Ion Research Facility in Lanzhou (HIRFL). JINST **15**, T12015 (2020). https://doi.org/10.1088/1748-0221/15/12/T12015
19. S.A. Voloshin, A.M. Poskanzer, R. Snellings, Collective phenomena in non-central nuclear collisions. Landolt-Bornstein **23**, 293–333 (2010). https://doi.org/10.1007/978-3-642-01539-710
20. S. Voloshin, Y. Zhang, Flow study in relativistic nuclear collisions by Fourier expansion of Azimuthal particle distributions. Z. Phys. C **70**, 665–672 (1996). https://doi.org/10.1007/s002880050141
21. R.J.M. Snellings, H. Sorge, S.A. Voloshin et al., Novel rapidity dependence of directed flow in high-energy heavy-ion collisions. Phys. Rev. Lett. **84**, 2803–2805 (2000). https://doi.org/10.1103/PhysRevLett.84.2803
22. J. Brachmann, S. Soff, A. Dumitru et al., Antiflow of nucleons at the softest point of the equation of state. Phys. Rev. C **61**, 024909 (2000). https://doi.org/10.1103/PhysRevC.61.024909
23. A.M. Poskanzer, S.A. Voloshin, Methods for analyzing anisotropic flow in relativistic nuclear collisions. Phys. Rev. C **58**, 1671–1678 (1998). https://doi.org/10.1103/PhysRevC.58.1671
24. M.I. Abdulhamid, B.E. Aboona, J. Adam et al., Measurement of directed flow in Au+Au collisions at $\sqrt{s_{\rm NN}} = 19.6$ and 27 GeV with the STAR event plane detector. Phys. Rev. C **111**, 014906 (2025). https://doi.org/10.1103/PhysRevC.111.014906
25. C. Alt, T. Anticic, B. Baatar et al., Directed and elliptic flow of charged pions and protons in Pb+Pb collisions at 40*A* and 158*A* GeV. Phys. Rev. C **68**, 034903 (2003). https://doi.org/10.1103/PhysRevC.68.034903
26. A. Adare, S. Afanasiev, C. Aidala et al., Measurements of higher order flow harmonics in Au+Au collisions at $\sqrt{s_{\rm NN}} = 200$GeV. Phys. Rev. Lett. **107**, 252301 (2011). https://doi.org/10.1103/PhysRevLett.107.252301
27. B.I. Abelev, M.M. Aggarwal, Z. Ahammed et al., Centrality dependence of charged hadron and strange hadron elliptic flow from $\sqrt{s_{\rm NN}} = 200$ GeV Au+Au collisions. Phys. Rev. C **77**, 054901 (2008). https://doi.org/10.1103/PhysRevC.77.054901
28. B. Abelev, J. Adam, D. Adamová et al., Anisotropic flow of charged hadrons, pions and (anti-)protons measured at high transverse momentum in Pb–Pb collisions at $\sqrt{s_{\rm NN}}$=2.76 TeV. Phys. Lett. B **719**, 18–28 (2013). https://doi.org/10.1016/j.physletb.2012.12.066
29. M.S. Abdallah, B.E. Aboona, J. Adam et al., Centrality and transverse-momentum dependence of higher-order flow harmonics of identified hadrons in Au+Au collisions at $\sqrt{s_{\rm NN}} = 200$ GeV. Phys. Rev. C **105**, 064911 (2022). https://doi.org/10.1103/PhysRevC.105.064911
30. L. Adamczyk, J.K. Adkins, G. Agakishiev et al., Centrality dependence of identified particle elliptic flow in relativistic heavy ion collisions at $\sqrt{s_{\rm NN}} = 7.7 - 62.4$ GeV. Phys. Rev. C **93**, 014907 (2016). https://doi.org/10.1103/PhysRevC.93.014907
31. L. Adamczyk, J.K. Adkins, G. Agakishiev et al., Centrality and transverse momentum dependence of elliptic flow of multistrange hadrons and ϕ meson in Au+Au collisions at $\sqrt{s_{\rm NN}} = 200$GeV. Phys. Rev. Lett. **116**, 062301 (2016). https://doi.org/10.1103/PhysRevLett.116.062301
32. D. Guo, H. Xu, D. Qi et al., The trigger system for the HIRFL-CSR external-target experiment. JINST **19**, T02018 (2024). https://doi.org/10.1088/1748-0221/19/02/T02018
33. Y. Chen, W. You, J. Lu et al., Design of a large-scale superconducting dipole magnet for the CEE spectrometer. Nucl. Instrum. Methods A **1074**, 170324 (2025). https://doi.org/10.1016/j.nima.2025.170324
34. J. Lu, Y. Chen, E. Mei et al., Structural design and test of superconducting magnet coil for the cooling storage ring external-target experiment. Supercond. Sci. Technol. **37**, 125013 (2024). https://doi.org/10.1088/1361-6668/ad85fd
35. Y. Yang, Z. Qin, Z. Li et al., A miniature prototype of time projection chambers for CSR external-target experiment. JINST **19**, T04007 (2024). https://doi.org/10.1088/1748-0221/19/04/T04007
36. W. Huang, F. Lu, H. Li et al., Laser test of the prototype of CEE time projection chamber. Nucl. Sci. Tech. **29**, 41 (2018). https://doi.org/10.1007/s41365-018-0382-4
37. X. Wang, D. Hu, M. Shao et al., CEE inner TOF prototype design and preliminary test results. JINST **17**, P09023 (2022). https://doi.org/10.1088/1748-0221/17/09/P09023
38. Y. Zhou, D. Hu, X. Wang et al., R & D of prototype iTOF-MRPC at CEE. Nucl. Instrum. Methods A **1054**, 168455 (2023). https://doi.org/10.1016/j.nima.2023.168455
39. Z.B. He, Z. Qin, P. Ma et al., Development of a MWDC prototype of the CSR external-target experiment. Nucl. Sci. Tech. **35**, 174 (2024). https://doi.org/10.1007/s41365-024-01515-0
40. Z. Qin, Z.B. He, Z. Cao et al., Beam test results of the prototype of the multi wire drift chamber for the CSR external-target experiment. Nucl. Sci. Tech. **36**, 67 (2025). https://doi.org/10.1007/s41365-024-01628-6
41. L.M. Lyu, H. Yi, L.M. Duan et al., Simulation and prototype testing of multi-wire drift chamber arrays for the CEE. Nucl. Sci. Tech. **31**, 11 (2020). https://doi.org/10.1007/s41365-019-0716-x
42. H. Yi, Z. Zhang, Z.G. Xiao et al., Prototype studies on the forward MWDC tracking array of the external target experiment at HIRFL-CSR. Chin. Phys. C **38**, 126002 (2014). https://doi.org/10.1088/1674-1137/38/12/126002
43. B. Wang, D. Han, Y. Wang et al., The CEE-eTOF wall constructed with new sealed MRPC. JINST **15**, C08022 (2020). https://doi.org/10.1088/1748-0221/15/08/C08022
44. B. Wang, H. Xu, K. Sun et al., Beam test result of the sealed MRPC prototype for CEE-eTOF. JINST **18**, C11001 (2023). https://doi.org/10.1088/1748-0221/18/11/C11001
45. S. Zhu, H. Yang, H. Pei et al., Prototype design of readout electronics for zero degree calorimeter in the HIRFL-CSR external-target experiment. JINST **16**, P08014 (2021). https://doi.org/10.1088/1748-0221/16/08/P08014
46. B. Zhang, L.K. Liu, H. Pei et al., Classifier for centrality determination with zero-degree calorimeter at the cooling-storage-ring external-target experiment. Nucl. Sci. Tech. **34**, 176 (2023). https://doi.org/10.1007/s41365-023-01338-5

47. D. Hu, M. Shao, Y. Sun et al., A T0/trigger detector for the external target experiment at CSR. JINST **12**, C06010 (2017). https://doi.org/10.1088/1748-0221/12/06/C06010
48. D. Hu, J. Lu, J. Zhou et al., Extensive beam test study of prototype MRPCs for the T0 detector at the CSR external-target experiment. Eur. Phys. J. C **80**, 282 (2020). https://doi.org/10.1140/epjc/s10052-020-7804-2
49. H.L. Wang, Z. Wang, C.S. Gao et al., Design and tests of the prototype a beam monitor of the CSR external target experiment. Nucl. Sci. Tech. **33**, 36 (2022). https://doi.org/10.1007/s41365-022-01021-1
50. J. Liu, C.S. Gao, H.L. Wang et al., Readout electronics for beam monitor in the external-target experiment of CSR. Nucl. Sci. Tech. **36**, 87 (2025). https://doi.org/10.1007/s41365-025-01652-0
51. Y. Nara, T. Maruyama, H. Stoecker, Momentum-dependent potential and collective flows within the relativistic quantum molecular dynamics approach based on relativistic mean-field theory. Phys. Rev. C **102**, 024913 (2020). https://doi.org/10.1103/PhysRevC.102.024913
52. Y. Nara, JAM: an event generator for high energy nuclear collisions. EPJ Web Conf. **208**, 11004 (2019). https://doi.org/10.1051/epjconf/201920811004
53. H. Sorge, Flavor production in Pb (160-A/GeV) on Pb collisions: effect of color ropes and hadronic rescattering. Phys. Rev. C **52**, 3291–3314 (1995). https://doi.org/10.1103/PhysRevC.52.3291
54. H. Liu, D. Zhang, S. He et al., Light nuclei production in Au+Au collisions at $\sqrt{s_{\rm NN}} = 5 - 200$ GeV from JAM model. Phys. Lett. B **805**, 135452 (2020). https://doi.org/10.1016/j.physletb.2020.135452
55. L.K. Liu, H. Pei, Y.P. Wang et al., Event plane determination from the zero degree calorimeter at the cooling storage ring external-target experiment. Nucl. Sci. Tech. **34**, 100 (2023). https://doi.org/10.1007/s41365-023-01262-8
56. J. Barrette, R. Bellwied, S. Bennett et al., Proton and pion production relative to the reaction plane in Au + Au collisions at 11 *A*GeV/*c*. Phys. Rev. C **56**, 3254–3264 (1997). https://doi.org/10.1103/PhysRevC.56.3254
57. M. Abdallah, B. Aboona, J. Adam et al., Disappearance of partonic collectivity in $\sqrt{s_{\rm NN}} = 3$ GeV Au+Au collisions at RHIC. Phys. Lett. B **827**, 137003 (2022). https://doi.org/10.1016/j.physletb.2022.137003
58. N. Borghini, P.M. Dinh, J.Y. Ollitrault et al., Effects of momentum conservation on the analysis of anisotropic flow. Phys. Rev. C **66**, 014901 (2002). https://doi.org/10.1103/PhysRevC.66.014901